Published in final edited form as:
Biol Psychiatry. 2014 August 1; 76(3): 203–212. doi:10.1016/j.biopsych.2013.12.009.

Antidepressant-like effects of cortical deep brain stimulation coincide with pro-neuroplastic adaptations of serotonin systems

Avin Veerakumar[1,2], **Collin Challis**[1,3], **Preetika Gupta**[1,3], **Jennifer Da**[1], **Aseem Upadhyay**[1], **Sheryl G. Beck**[3,4], and **Olivier Berton**[1,3]

[1]. Department of Psychiatry, Perelman School of Medicine, University of Pennsylvania, Philadelphia, PA 19104

[2]. Department of Bioengineering, University of Pennsylvania, Philadelphia, PA 19104

[3]. Neuroscience Graduate Group, Perelman School of Medicine, University of Pennsylvania, Philadelphia, PA 19104

[4]. Department of Anesthesiology, Children's Hospital of Philadelphia Research Institute and Perelman School of Medicine, University of Pennsylvania, Philadelphia, PA 19104

Abstract

Background—Cortical deep brain stimulation (DBS) is a promising therapeutic option for treatment-refractory depression but its mode of action remains enigmatic. Serotonin (5-HT) systems are engaged indirectly by ventromedial prefrontal cortex (vmPFC) DBS. Resulting neuroplastic changes in 5-HT systems could thus coincide with the long-term therapeutic activity of vmPFC DBS.

Methods—We tested this hypothesis by evaluating the antidepressant-like activity of vmPFC DBS in the chronic social defeat stress (CSDS) model of depression (n = 8-13 mice per group). Circuit-wide activation induced by vmPFC DBS was mapped using c-Fos immunolabeling. The effects of chronic vmPFC DBS on the physiology and morphology of genetically-identified 5-HT cells from the Dorsal Raphe Nucleus (DRN) were examined using whole-cell recording, somatodendritic 3-D reconstructions and morphometric analyses of presynaptic boutons along 5-HT axons.

Results—Acute DBS drove c-Fos expression locally in the vmPFC and in several distal monosynaptically-connected regions, including the DRN. Chronic DBS reversed CSDS-induced

Corresponding Author: Olivier Berton 125 S 31st Street, TRL Building, Room 2218 Philadelphia, PA 19104-3403 bertonol@mail.med.upenn.edu (215)-573-2041.

Author Contributions

A.V. and O.B. designed research; A.V., C.C., P.G., J. D., and A.U. performed research; A.V., C.C., S.G.B., and O.B. analyzed data; A.V., C.C., and O.B wrote the paper.

FINANCIAL DISCLOSURES

The authors report no biomedical financial interests or potential conflicts of interest.

social avoidance, restored the disrupted balance of excitatory/inhibitory inputs onto 5-HT neurons, and reversed 5-HT hypoexcitability observed after CSDS. Furthermore, vmPFC DBS reversed CSDS-induced arborization of 5-HT dendrites in the DRN and increased the size and density of 5-HT presynaptic terminals in the dentate gyrus and vmPFC.

Conclusions—We validate a new preclinical paradigm to examine cellular mechanisms underlying the antidepressant-like activity of vmPFC DBS and identify dramatic circuit-mediated cellular adaptations which coincide with this treatment. These neuroplastic changes of 5-HT neurons may contribute to the progressive mood improvements reported in patients treated with chronic courses of cortical DBS.

Keywords

Deep Brain Stimulation; Depression; Dorsal Raphe; Prefrontal Cortex; Neuroplasticity; Social Defeat

INTRODUCTION

Deep brain stimulation (DBS) of the subcallosal cingulate gyrus (SCG) has demonstrated promise as a somatic therapy for treatment-refractory depression (1-3). Clinical evidence suggests that the antidepressant effects of SCG DBS are reinforced by chronic stimulation, with the fraction of remitters increasing linearly over months of DBS treatment (3), raising the possibility that long-term neuroadaptations are important contributors to its therapeutic activity. However, the existence and neurobiological nature of such changes remains enigmatic.

To date only a handful of studies have examined the behavioral and neurobiological effects of DBS of the ventromedial prefrontal cortex (vmPFC) (the rodent analog of the SCG) in preclinical models. Most of these studies have applied acute stimulation regimens and reported antidepressant-like effects in behavioral screens sensitive to pharmacological antidepressants (4,5). The observation that serotonin (5-hydroxytryptamine, 5-HT) depletion blocks the behavioral effects of acute and chronic DBS suggests that engagement of an intact serotonergic (5-HT) system is required for the antidepressant-like activity of DBS in rats (6,7).

Neuroanatomical tracing studies in rodents and primates indicate that the Dorsal Raphe Nucleus (DRN) receives projections from the vmPFC (8-11) and several preclinical studies have reported robust and immediate increases in DRN neural activity and serotonin output upon electrical or optogenetic stimulation of the vmPFC (6,9,10,12-14). Whether and how chronic regimens of vmPFC DBS induce neuroplasticity in the 5-HT system is not known. Because previous studies have indicated that depression and suicide in humans (15-18) and depressive-like symptoms in animals (19-21) are accompanied by maladaptive plasticity in the 5-HT system, we hypothesized that stable neuroplastic changes in the 5-HT system may coincide with the antidepressant-like effect of chronic vmPFC DBS.

To test this hypothesis we assessed the effects of chronic vmPFC DBS in mice in the context of a chronic social defeat stress (CSDS) paradigm that has face and predictive validity with

regard to clinical depression (22,23). We first assessed the ability of chronic vmPFC DBS to suppress CSDS-induced social avoidance and used c-Fos immunolabeling to map the regions in which DBS was inducing neural activity. We then used a transgenic mouse line allowing for genetic identification and conditional viral targeting of 5-HT cells, together with an array of electrophysiological and morphological assays, to investigate whether chronic vmPFC DBS reversed defeat-induced changes in the structure and physiology of DRN 5-HT neurons. We report that chronic vmPFC DBS abolishes social avoidance behavior after CSDS and induces dramatic physiological, dendritic, and axonal neuroplastic adaptations in DRN 5-HT neurons that counteract the maladaptive adaptations induced by CSDS.

METHODS AND MATERIALS

Animals

8-12 week old male wild-type (for behavior and c-Fos experiments) or *Pet1-tdTomato* transgenic mice (for electrophysiology and morphology experiments) bred onto a C57BL/6 background were used for all experiments (generation of transgenic mice is described in Supplement 1). Mice were housed on a 12 hour light/dark cycle with food and water available *ad libitum*, except during DBS or sham stimulation. All studies were conducted strictly according to protocols approved by the University of Pennsylvania Institutional Animal Care and Use Committee, and all procedures were performed in accordance with institutional guidelines.

Social Defeat and Social Interaction Testing

Social defeat and social interaction testing were conducted as previously reported (20-23) and described in detail in Supplement 1. Briefly, mice underwent 10 days of aggression stress from trained CD1 aggressor mice. For social interaction tests, mice were allowed to freely explore an arena for 2.5 minutes in the absence of a novel social target, and for 2.5 minutes in the presence of a novel social target; stress susceptible mice develop a persistent social avoidance, as indicated by a decreased time spent in the "interaction zone" around the social target (22). In all DBS experiments, only defeated mice which expressed social avoidance (i.e. stress-susceptible) were stimulated. Individual mice were assigned randomly to the "Defeat Sham" or "Defeat Stim" conditions on Day 11 such that the two groups had comparable mean avoidance scores before DBS treatment. "Control" mice were handled identically to defeated mice but were not subjected to aggression stress.

DBS Surgeries

Stainless steel, 125 μm diameter, 4 mm length bipolar electrodes (Plastics One, Roanoke, VA) were lowered at a 15° angle and implanted unilaterally into the left vmPFC [1.8 mm anteroposterior (AP), 0.8 mm mediolateral (ML), −0.27 mm dorsoventral (DV)] over a 5 minute time period. Coordinates were adopted from previous reports such that the electrode tips would be localized to the junction of the prelimbic and infralimbic cortex (21,24). Cyanoacrylate and dental cement were used to affix electrodes to the skull as previously described (25). Sham-stimulated mice were implanted identically. One mouse was removed from all analyses due to electrode placement outside the vmPFC, and one mouse was

removed from all analyses due to excessive tissue damage such that the electrode placement could not be determined.

DBS Experiments

After a one week recovery from surgery, implanted electrodes were connected to a programmable stimulator (MED Associates, St. Albans, VT). Stimulation was applied at 160 Hz frequency, 60 μs pulse width, and 150 μA current, parameters which are similar to previous DBS studies in rodents and humans (1,6,26-28). For c-Fos expression experiments, mice were stimulated for 1 hour immediately followed by perfusion. For chronic DBS experiments, DBS was applied 5 hours per day for 7 days—a paradigm similar to prior chronic DBS studies for depression which have observed long-lasting antidepressant-like effects (7,29-31)—while mice remained in their home cages. Sham-stimulated mice were handled and connected to the stimulator in an identical manner, but no current was applied. Following 7 days of DBS, mice underwent social interaction testing 24 hours after the end of stimulation (mice were not stimulated during testing). To determine electrode placements, mice were perfused 24 hours after the conclusion of social interaction testing. For electrophysiology experiments, mice were sacrificed 24 hours following the final social interaction test. For axonal morphology experiments, mice were perfused 24 hours following the conclusion of DBS.

Histology and Immunohistochemistry

To visualize c-Fos, PSD-95, and Synaptophysin-Venus (SynP-Venus) by immunohistochemistry, brain slices were processed for immunohistochemistry using standard protocols (20,21). Histology, antibodies, incubation times, and imaging and quantification details are described in Supplement 1.

Whole-Cell Electrophysiology

200 μm coronal slices containing the DRN were used for whole cell recording and prepared as described previously (20,21,32-34). 5-HT cells from the ventromedial DRN (vmDRN) were recorded (32). Detailed electrophysiology and data analysis protocols can be found in Supplement 1.

Morphometric analyses of somatodendritic structure and axonal boutons of 5-HT neurons

To analyze somatodendritic morphology, genetically identified 5-HT neurons from *Pet1-tdTomato* mice were filled with 1% biocytin during whole-cell recording and were analyzed as described previously (20) using Neurolucida software (MBF Bioscience, Williston, VT) and described in Supplement 1.

For morphometric analyses of presynaptic boutons along 5-HT axons, we applied a cell-type specific genetic tagging approach that relies on a fluorescently-labeled form of the presynaptic protein synaptophysin (Synaptophysin-Venus) which we expressed selectively in DRN 5-HT neurons using a conditional viral vector injected seven days prior to the beginning of CSDS. Following CSDS, DBS, and perfusion, brain slices were stained with anti-GFP antibodies. In addition to the DRN, the dentate gyrus (DG), vmPFC, basolateral amygdala (BLA), were selected for a subsequent detailed morphometric analysis based on

their innervation by DRN neurons and differential activation in response to vmPFC DBS. Bouton length and bouton density were measured as described in Supplement 1 and Figure S3. These two variables have been previously validated as sensitive indices of axonal plasticity, including in serotonin neurons (35-37). A total of 7853 boutons were analyzed out of 425 axons representing a cumulated axon length of approximately 30000 μM.

Statistical Methods

One-way, two-way, or repeated measures ANOVAs were performed, followed by post-hoc comparisons using Fisher's PLSD test. Comparisons between two groups were performed by two-tailed Student's *t*-tests. Statistical analyses were performed using Statistica software (StatSoft, Tulsa, OK). Statistical significance was defined as $p < 0.05$. All data are presented as the mean ± SEM. Outlying values (3 standard deviations from the mean) were excluded from group means.

RESULTS

Antidepressant-like effect of chronic vmPFC DBS in stress-susceptible mice

We first investigated the behavioral effect of chronic vmPFC DBS in the CSDS paradigm (Figure 1A). Histological analyses confirmed that DBS electrodes were placed in the vmPFC during experiments (Figure 1B). A social interaction test conducted on Day 11 prior to surgery verified that interaction times were decreased in defeat-susceptible mice (Main Effect of Defeat $F_{(1,6)} = 167.11$, $p = 4.33*10^{-15}$) (Figure 1C, Left). When social interaction was retested on Day 25 following 7 days of chronic vmPFC DBS, defeated, sham-stimulated mice still expressed social avoidance at a level that did not differ significantly from Day 11 (Main Effect of CSDS at Day 25 $F_{(1,35)} = 4.78$, $p = 0.03$). In contrast, DBS dramatically increased social interaction scores, restoring social interaction to levels similar to unstressed controls on Day 25 (Defeat x Stimulation interaction: $F_{(1,35)} = 6.29$, $p = 0.0169$). (Figure 1C,D). In the absence of a social target, DBS had no effect on interaction times (Figure S1A,B). DBS non-specifically increased total distance traveled regardless of treatment condition or the presence of a social target (Day 25 Target Absent: Main effect of Stimulation $F_{(1,36)} = 6.47$, $p = 0.02$, Day 25 Target Present: Main effect of Stimulation $F_{(1,36)} = 9.80$, $p = 0.003$) (Figure S1C-F).

Acute vmPFC DBS induces c-Fos expression in brain regions with afferent and efferent monosynaptic connections

To identify distal regions modulated by vmPFC DBS, we applied 1 hour of DBS to the vmPFC of naïve mice (Figure 2A) and conducted a brain-wide examination of c-Fos induction. An initial survey identified several regions with marked c-Fos induction or lack thereof, a subset of which were selected for subsequent blinded quantitative assessment, including the vmPFC, the anterior piriform cortex (Pir) (an input region to the IL in mice, Figure S2), the DG (which does not receive or send direct inputs to the vmPFC), the lateral habenula (LHb) (an output region of the vmPFC), and the basolateral amygdala (BLA) and DRN (two reciprocal input and ouput regions of the vmPFC) (11,38). As expected, acute DBS increased c-Fos immunoreactivity locally in the vmPFC (Student's *t*-test, $p < 0.01$)

(Figure 2B-C). vmPFC DBS also increased c-Fos counts in the Pir, LHb, BLA, and DRN ($p < 0.05$), while c-Fos levels in the DG did not significantly increase ($p > 0.05$) (Figure 2B-C).

Chronic DBS reverses CSDS-induced desensitization of 5-HT neurons and restores normal levels of inhibitory input

Our previous studies have demonstrated that CSDS sensitizes synaptic inhibitory inputs and drives a state of sustained intrinsic hypoexcitability of DRN 5-HT neurons in susceptible but not resilient mice (20,21,34). To determine whether chronic vmPFC DBS counteracts such stress-induced changes, we performed whole cell recordings in DRN slices collected 48 hours following the cessation of DBS administration (Figure 3A-B). Consistent with our previous reports, we found that CSDS decreased the intrinsic excitability of DRN 5-HT neurons (Figure 3C,E). DBS reversed CSDS-induced hypoexcitability, restoring intrinsic excitability of DRN 5-HT cells to the levels of unstressed sham controls. (Treatment x Input Current interaction, $F_{(6,341)} = 3.27$, $p < 0.001$; Figure 3C,E). CSDS also raised the action potential threshold to a more depolarized state, while DBS reverses this effect (One-Way ANOVA, $F_{(2,61)} = 4.06$, $p = 0.023$; Figure 3F).

We next tested whether chronic vmPFC DBS affects the excitatory and inhibitory synaptic inputs onto DRN 5-HT neurons using voltage clamp techniques (34,39). As previously observed (21), CSDS increased spontaneous IPSC frequency of 5-HT neurons in susceptible mice (One-Way ANOVA: $F_{(2,39)} = 6.55$, $p = 0.004$, Figure 3D, inset of Figure 3H). DBS reversed this potentiation, returning inhibitory input to the levels of controls (Kolmogorov-Smirnov test, $Z = 11.44$, $p < 0.001$; Figure 3H). Following CSDS, there was a trend towards a decreased IPSC amplitude in the Defeat Sham (20.77 ± 1.99 pA) and Defeat Stim (19.66 ± 1.11 pA) groups when compared to the Control Sham group (25.59 ± 4.5 pA), but this difference was not significant. We next analyzed EPSC frequency of DRN 5-HT neurons and found that CSDS did not affect this variable. Interestingly, we observed a sustained enhancement of EPSC frequency by DBS treatment (One-Way ANOVA, $F_{(2,39)} = 7.65$, $p = 0.002$; Figure 3I).

Chronic vmPFC DBS induces dendritic plasticity in DRN 5-HT neurons

Consistent with our previous work (20), we found that CSDS increased the length and branching complexity of dendrites of DRN 5-HT neurons which were filled during patch clamp recordings (Mean Dendrite Length: $F_{(2,38)} = 9.33$, $p = 0.001$, Figure 4A,B; Sholl Intersections: $F_{(2,38)} = 8.49$, $p = 0.001$, Figure 4A,C). DBS reversed these CSDS-induced dendritic adaptations, restoring dendritic length and complexity to control levels (Defeat Sham *vs.* Defeat Stim, $p < 0.01$ for dendrite length and $p < 0.01$ for Sholl intersections). DBS also restored total dendritic length to the level of controls ($F_{(2,38)} = 5.19$, $p = 0.01$). Furthermore, in line with our observation that DBS increases excitatory input onto DRN 5-HT neurons, immunolabeling for the excitatory postsynaptic density marker PSD-95 revealed a significant enhancement of the number of postsynaptic densities per micron of DRN tdTomato$^+$ process (One-Way ANOVA, $F_{(2,45)} = 10.54$, $p < 0.001$; Figure 4D,E). Importantly, the number of PSD-95 puncta per micron of 5-HT dendrite was not altered by CSDS.

Social defeat and chronic vmPFC DBS induce axonal plasticity in DRN 5-HT neurons

Previous studies have implicated the stimulation of 5-HT release in DRN projection regions such as the hippocampus as a possible mechanism of action of vmPFC DBS (5,7). Because serotonin is released both synaptically and extrasynaptically from synaptic boutons and axonal varicosities (40), which are dynamic structures (36,37,41,42), we sought to investigate whether CSDS and/or DBS induce sustained changes in the morphology or density of boutons along the axons of DRN 5-HT neurons. To visualize axons and boutons originating from DRN 5-HT neurons, *Pet1-tdTomato* mice were injected in the DRN with a Cre-dependent adeno-associated virus (AAV) expressing SynP-Venus and underwent CSDS and DBS (Figure 5A,B). Over 99% of SynP-Venus-expressing somas in the DRN also expressed tdTomato, confirming 5-HT-selective transgene expression. Approximately 40% of 5-HT neurons in the DRN were labeled at the site of injection, indicating robust transduction efficiency (Figure 5C,D). Transduction rates were not significantly different between experimental groups (One-Way ANOVA, $F_{(2,9)} = 0.554$, $p > 0.05$, Figure 5D). While infected cell bodies were only observed in the DRN, fluorescent puncta typical of presynaptic labeling were observed broadly in the brainstem, outside of the site of injection, as well as widely throughout the forebrain. The regional pattern was similar to that of serotonergic innervation and co-localized with serotonin (not shown) and tdTomato in axon terminals, indicating that the tagged protein was effectively targeted to 5-HT presynaptic structures in remote regions innervated by the DRN (Figure 5C).

In the DG and vmPFC of sham-treated mice, CSDS induced significant reductions of the average length and density of presynaptic boutons along DRN 5-HT axons (Figure 5E,F) (Main effect on DG bouton length: $F_{(2,2000)} = 21.37$, $p < 0.001$, effect on DG bouton density: $F_{(2,119)} = 10.64$, $p < 0.001$, effect on vmPFC bouton length: $F_{(2,3046)} = 21.741$, $p < 0.001$, effect on vmPFC bouton density: $F_{(2,177)} = 6.55$, $p < 0.001$; Figure 5H,I,K,L). DBS restored bouton length to levels comparable to unstressed controls in the DG and vmPFC (Figure 5E,F,H,I), and restored bouton density to control levels in the DG (**Figure E,K**). Surprisingly, in contrast to its effects in the DG and the vmPFC, CSDS did not alter bouton length and it increased bouton density in the BLA ($F_{(2,120)} = 3.891$, $p = 0.0231$) (Figure 5G,J,M). In this region, DBS increased bouton length over the level of controls, ($F_{(2,2798)} = 25.68$, $p < 0.001$) and did not change bouton density. All DBS-induced changes in bouton length were reflected in a leftward shift of cumulative probability plots after CSDS (Figure 5H,I,J) (Kolmogorov-Smirnov Test, $p < 0.01$ in DG, vmPFC, and BLA).

DISCUSSION

In this study we have demonstrated that chronic vmPFC DBS reverses social avoidance in a mouse model of depression and induces striking neuroadaptations in brainstem 5-HT neurons which reverse CSDS-induced maladaptive plasticity and point to a sustained increase in 5-HT activity upon repeated courses of DBS.

We first built on previous studies of cortical DBS in the chronic mild stress model (7,31) by demonstrating the efficacy of DBS in modulating CSDS-induced social avoidance, which models another symptom of human depression. In line with our previous reports (20-22) CSDS induced a persistent social withdrawal. Seven days of unilateral chronic vmPFC DBS

proved sufficient to restore social approach behavior to levels comparable to unstressed mice. The finding that left unilateral DBS was sufficient to elicit an antidepressant-like responses is consistent with previous observations that stimulation of the left vmPFC or left LHb is sufficient to produce antidepressant-like responses in the forced swim test (43) and the learned helplessness paradigm (44). Furthermore, we found that chronic DBS stimulated social interaction in defeated, stress-susceptible mice while it had no effects on social interaction in unstressed mice, which is consistent with previous work indicating that the effect of DBS is observed in stressed but not control rats (7). The effects of DBS on approach behavior were specific to a social target, and this antidepressant-like effect were superimposed on a small, non-specific locomotor stimulant effect of DBS that was seen in all animals independently of their previous exposure to social stress, which is consistent with clinical results indicating that SCG DBS increases motor speed (1). It should be noted that the CSDS and interaction test paradigm used in these experiments has some limitations as a model of depression, as anhedonic-like behavior following CSDS is short-lived (45) compared to social avoidance, and the behavioral sequelae of CSDS may generalize to other disorders such as anxiety and PTSD (46).

SCG DBS has been shown to modulate the activity of remote brain regions in human PET studies (2), and prior preclinical studies report activation of the DRN, a well characterized target of vmPFC projection neurons (13,14). To further characterize the regions modulated by vmPFC DBS, we examined circuit-wide c-Fos expression after acute vmPFC DBS. DBS drove local neural activity in the vmPFC, which is consistent with preclinical studies showing that DBS also increased local c-Fos levels when applied in the NAc (30), NAc shell (27,28), and LHb (44). Consistent with DBS-induced orthodromic activation, we observed significant c-Fos activation in the LHb, BLA, and DRN. Activation of the LHb indicates that vmPFC DBS may indirectly engage a similar circuit mechanism to LHb DBS, which is also being explored as a treatment for depression (47). DRN activation could provide an explanation for increased hippocampal 5-HT release with vmPFC DBS (6). We observed robust c-Fos activation in the anterior piriform cortex (Pir), an input region to the vmPFC. This activation may occur through DBS-induced antidromic transmission, which is consistent with recent findings from DBS of the NAc shell (28) and a large body of data from DBS of the subthalamic nucleus (48). As expected, we did not observe significant activation in the DG, which neither receives nor sends projections to the vmPFC (11,38).

In agreement with our previous findings (20,21), CSDS decreased cellular excitability, increased inhibitory input, and increased dendritic length and complexity in DRN 5-HT neurons. Importantly, in the present study these observations were made 14 days following the end of CSDS compared to 24 hours post-CSDS in our previous studies, indicating that CSDS-induced changes in physiology and morphology are highly stable. Chronic vmPFC DBS restored DRN 5-HT intrinsic excitability, action potential threshold, and inhibitory input to levels comparable to undefeated controls, indicating a dramatic DBS-mediated reversal of CSDS-induced maladaptive plasticity. The combined resensitization and shift in the balance of excitatory/inhibitory synaptic inputs onto 5-HT neurons may play a causal role in the restoration of social approach behaviors. Indeed, a recent study demonstrated that direct stimulation of glutamatergic vmPFC-DRN axons promoted antidepressant responses (13). Furthermore we have recently shown that optogenetic silencing of DRN GABAergic

neurons that receive inputs from the vmPFC and monosynaptically inhibit nearby 5-HT cells blocks the consolidation of social avoidance during CSDS (21). Though the precise cellular mechanisms responsible for these adaptations remain unknown, our morphological analyses point to a number of possible underlying mechanisms. In other types of neurons, intrinsic excitability and firing pattern has been shown to be causally related to dendritic morphology, size and topology (49). The reduction in dendritic length and complexity observed after DBS administration may thus mediate changes in excitability. Interestingly, we also observed a strengthening of excitatory synaptic input onto DRN 5-HT neurons, a variable that was not initially altered by CSDS. This could be attributed to an increase in the number of excitatory synapses or an increased presynaptic release probability. We observed a DBS-induced increase in the density of PSD-95^{+} puncta along DRN 5-HT dendrites, indicating that the former may be the case. Indeed, it has been shown that PSD-95 overexpression increases mEPSC frequency and decreases inhibitory synaptic input (50), both of which were observed in DRN 5-HT neurons following chronic DBS in this study. The finding that inhibitory synaptic input was restored by chronic vmPFC DBS raises the possibility of DBS-induced plasticity in DRN GABA neurons; indeed, prior electrophysiological and structural evidence indicates that most vmPFC-DRN afferents synapse onto non-5-HT neurons (10,12,51), and we have previously shown that in defeated mice, maladaptive plasticity in DRN GABA neurons coincides with maladaptive plasticity in DRN 5-HT neurons (21).

Because CSDS and chronic vmPFC DBS induced physiological and dendritic morphological adaptations in DRN 5-HT neurons, we asked whether DBS also induces adaptations in DRN 5-HT axons that may translate into altered synaptic output in innervated regions. We achieved cell-type specific anterograde labeling of DRN 5-HT axons and selectively visualized their presynaptic boutons in forebrain projections regions for morphometric analysis. This approach is advantageous over previous methods used to detect axons of 5-HT cells that rely on conventional tracers or endogenous markers such as 5-HT or 5-HTT, as such approaches may detect a large proportion of varicosities that do not to form functional synapses and which possibly originate from non-5-HT neurons in the DRN.

We used our approach to demonstrate that CSDS has a significant effect on both the density and/or length of 5-HT varicosities in all regions examined. CSDS induced a decrease in the length and density of boutons in the DG and vmPFC, suggesting a decrease in the strength and number of functional 5-HT synapses. DBS restored bouton length and density in the DG and restored bouton length in the vmPFC, suggesting that repeated DBS may reinforce 5-HT output to the hippocampus and vmPFC by concomitantly increasing 5-HT firing along with the number and size of release sites. DBS-induced effects on 5-HT bouton dynamics were region- and projection-specific; we observed that CSDS exerted an opposing influence on bouton density in the BLA as compared to the DG and vmPFC. This observation is in line with previous findings that stress induces opposing neuroplastic changes in the BLA and DG (52).

Mechanisms leading to increased boutons are unclear. Recent studies suggest that the dynamics of varicosities reflect localized neuronal activity. After high frequency electrical stimulation, increases in bouton density were observed selectively on axons that are in the

microproximity of c-Fos$^+$ neuronal somas (36). Such mechanisms could explain the increases observed in the vmPFC and BLA, but would not account for changes in the DG, since this region was not noticeably activated by DBS. Axonal adaptations in the DG are suggestive of somatodendritic engagement of 5-HT neurons and consecutive effects on nuclear translation and axonal transport. Further studies will be necessary to establish the molecular underpinnings of these adaptations. This is to our knowledge the first investigation of 5-HT presynaptic bouton dynamics in the context of depression or vmPFC DBS.

Overall, our study establishes a novel experimental paradigm that may prove advantageous to assess cell-type specific mechanisms of DBS using transgenic mouse lines, and we identify DRN 5-HT neurons as a key neural substrate for further studies on the long-term mechanisms of SCG DBS in depression.

Supplementary Material

Refer to Web version on PubMed Central for supplementary material.

Acknowledgments

The authors acknowledge Janette Boulden for excellent technical assistance, R. Christopher Pierce and Fair M. Vassoler for providing DBS equipment, and Casey H. Halpern for advice on surgical techniques. This work was supported by the National Institutes of Health (National Institute of Mental Health Grants #MH087581 to O.B. and Grants #MH0754047 and #MH089800 to S.G.B. and National Research Service Award Grants #T32MH014654 and #F31MH097386 to C.C.), the International Mental Health Research Organization (O.B.), the National Alliance for Research in Schizophrenia and Affective Disorders (O.B.).

REFERENCES

1. Mayberg HS, Lozano AM, Voon V, McNeely HE, Seminowicz D, Hamani C, et al. Deep brain stimulation for treatment-resistant depression. Neuron. 2005; 45:651–60. [PubMed: 15748841]
2. Lozano AM, Mayberg HS, Giacobbe P, Hamani C, Craddock RC, Kennedy SH. Subcallosal cingulate gyrus deep brain stimulation for treatment-resistant depression. Biological Psychiatry. 2008; 64:461–7. [PubMed: 18639234]
3. Holtzheimer PE, Kelley ME, Gross RE, Filkowski MM, Garlow SJ, Barrocas A, et al. Subcallosal cingulate deep brain stimulation for treatment-resistant unipolar and bipolar depression. Archives of General Psychiatry. 2012; 69:150–8. [PubMed: 22213770]
4. Hamani C, Nobrega JN. Preclinical Studies Modeling Deep Brain Stimulation for Depression. Biological Psychiatry. 2012; 72:916–923. [PubMed: 22748616]
5. Hamani C, Temel Y. Deep Brain Stimulation for Psychiatric Disease: Contributions and Validity of Animal Models. Science Translational Medicine. 2012; 4:1–12.
6. Hamani C, Diwan M, Macedo CE, Brandão ML, Shumake J, Gonzalez-Lima F, et al. Antidepressant-like effects of medial prefrontal cortex deep brain stimulation in rats. Biological Psychiatry. 2010; 67:117–24. [PubMed: 19819426]
7. Hamani C, Machado DC, Hipólide DC, Dubiela FP, Suchecki D, Macedo CE, et al. Deep brain stimulation reverses anhedonic-like behavior in a chronic model of depression: role of serotonin and brain derived neurotrophic factor. Biological Psychiatry. 2012; 71:30–5. [PubMed: 22000731]
8. Freedman L, Insel T, Smith Y. Subcortical projections of area 25 (subgenual cortex) of the macaque monkey. The Journal of Comparative Neurology. 2000; 421:172–88. [PubMed: 10813780]
9. Varga V, Székely A, Csillag A, Sharp T, Hajós M. Evidence for a role of GABA interneurones in the cortical modulation of midbrain 5-hydroxytryptamine neurones. Neuroscience. 2001; 106:783–792. [PubMed: 11682163]

10. Varga V, Kocsis B, Sharp T. Electrophysiological evidence for convergence of inputs from the medial prefrontal cortex and lateral habenula on single neurons in the dorsal raphe nucleus. European Journal of Neuroscience. 2003; 17:280–286. [PubMed: 12542664]
11. Vertes R. Differential projections of the infralimbic and prelimbic cortex in the rat. Synapse. 2004; 51:32–58. [PubMed: 14579424]
12. Celada P, Puig M, Casanovas J, Guillazo G, Artigas F. Control of Dorsal Raphe Serotonergic Neurons by the Medial Prefrontal Cortex: Involvement of Serotonin-1A, GABAA, and Glutamate Receptors. The Journal of Neuroscience. 2001; 21:9917–9929. [PubMed: 11739599]
13. Warden MR, Selimbeyoglu A, Mirzabekov JJ, Lo M, Thompson KR, Kim S, et al. A prefrontal cortex-brainstem neuronal projection that controls response to behavioural challenge. Nature. 2012; 492:428–32. [PubMed: 23160494]
14. Kumar S, Black SJ, Hultman R, Szabo ST, DeMaio KD, Jeanette du, et al. Cortical control of affective networks. The Journal of Neuroscience. 2013; 33:1116–29. [PubMed: 23325249]
15. Matthews P, Harrison P. A morphometric, immunohistochemical, and in situ hybridization study of the dorsal raphe nucleus in major depression, bipolar disorder, schizophrenia, and suicide. Journal of Affective Disorders. 2012; 137:125–34. [PubMed: 22129767]
16. Hercher C, Turecki G, Mechawar N. Through the looking glass: examining neuroanatomical evidence for cellular alterations in major depression. Journal of Psychiatric Research. 2009; 43:947–61. [PubMed: 19233384]
17. Budisic M, Mislav B, Karlovic D, Dalibor K, Trkanjec Z, Zlatko T, et al. Brainstem raphe lesion in patients with major depressive disorder and in patients with suicidal ideation recorded on transcranial sonography. European Archives of Psychiatry and Clinical Neuroscience. 2010; 260:203–8. [PubMed: 19756820]
18. Kerman IA, Bernard R, Bunney WE, Jones EG, Schatzberg AF, Myers RM, et al. Evidence for Transcriptional Factor Dysregulation in the Dorsal Raphe Nucleus of Patients with Major Depressive Disorder. Frontiers in Neuroscience. 2012; 6:135. [PubMed: 23087602]
19. Deneris E, Wyler S. Serotonergic transcriptional networks and potential importance to mental health. Nature Neuroscience. 2012; 15:519–27.
20. Espallergues J, Teegarden S, Veerakumar A, Boulden J, Challis C, Jochems J, et al. HDAC6 Regulates Glucocorticoid Receptor Signaling in Serotonin Pathways with Critical Impact on Stress Resilience. The Journal of Neuroscience. 2012; 32:4400–4416. [PubMed: 22457490]
21. Challis C, Boulden J, Veerakumar A, Espallergues J, Vassoler F, Pierce R, et al. Raphe GABAergic Neurons Mediate the Acquisition of Avoidance after Social Defeat. The Journal of Neuroscience. 2013; 33:13978–13988. [PubMed: 23986235]
22. Berton O, McClung CA, Dileone RJ, Krishnan V, Renthal W, Russo SJ, et al. Essential role of BDNF in the mesolimbic dopamine pathway in social defeat stress. Science. 2006; 311:864–8. [PubMed: 16469931]
23. Golden SA, Covington HE, Berton O, Russo SJ. A standardized protocol for repeated social defeat stress in mice. Nature Protocols. 2011; 6:1183–91.
24. Covington HE, Lobo MK, Maze I, Vialou V, Hyman JM, Zaman S, et al. Antidepressant effect of optogenetic stimulation of the medial prefrontal cortex. The Journal of Neuroscience. 2010; 30:16082–90. [PubMed: 21123555]
25. Agterberg MJ, Spoelstra EN, van der Wijst S, Brakkee JH, Wiegant VM, Hamelink R, et al. Evaluation of temperature rise and bonding strength in cements used for permanent head attachments in rats and mice. Laboratory Animals. 2010; 44:264–70. [PubMed: 20573682]
26. Vassoler FM, Schmidt HD, Gerard ME, Famous KR, Ciraulo DA, Kornetsky C, et al. Deep brain stimulation of the nucleus accumbens shell attenuates cocaine priming-induced reinstatement of drug seeking in rats. The Journal of Neuroscience. 2008; 28:8735–9. [PubMed: 18753374]
27. Halpern CH, Tekriwal A, Santollo J, Keating JG, Wolf JA, Daniels D, Bale TL. Amelioration of binge eating by nucleus accumbens shell deep brain stimulation in mice involves D2 receptor modulation. The Journal of Neuroscience. 2013; 33:7122–9. [PubMed: 23616522]
28. Vassoler FM, White SL, Hopkins TJ, Guercio LA, Espallergues J, Berton O, et al. Deep Brain Stimulation of the Nucleus Accumbens Shell Attenuates Cocaine Reinstatement through Local and

Antidromic Activation. The Journal of Neuroscience. 2013; 33:14446–14454. [PubMed: 24005296]

29. Falowski SM, Sharan A, Reyes BA, Sikkema C, Szot P, van Bockstaele EJ. An Evaluation of Neuroplasticity and Behavior After Deep Brain Stimulation of the Nucleus Accumbens in an Animal Model of Depression. Neurosurgery. 2011; 69:1281–1290. [PubMed: 21566538]
30. Schmuckermair C, Gaburro S, Sah A, Landgraf R, Sartori SB, Singewald N. Behavioral and neurobiological effects of deep brain stimulation in a mouse model of high anxiety- and depression-like behavior. Neuropsychopharmacology. 2013; 38:1234–44. [PubMed: 23325324]
31. Dournes C, Beeské S, Belzung C, Griebel G. Deep brain stimulation in treatment-resistant depression in mice: Comparison with the CRF1 antagonist, SSR125543. Progress in Neuro-Psychopharmacology and Biological Psychiatry. 2013; 40:213–220. [PubMed: 23367508]
32. Crawford LK, Craige CP, Beck SG. Increased Intrinsic Excitability of Lateral Wing Serotonin Neurons of the Dorsal Raphe: A Mechanism for Selective Activation in Stress Circuits. Journal of Neurophysiology. 2010; 103:2652–2663. [PubMed: 20237311]
33. Calizo LH, Akanwa A, Ma X, Pan Y, Lemos JC, Craige C, et al. Raphe serotonin neurons are not homogenous: electrophysiological, morphological and neurochemical evidence. Neuropharmacology. 2011; 61:524–43. [PubMed: 21530552]
34. Crawford LK, Rahman SF, Beck SG. Social Stress Alters Inhibitory Synaptic Input to Distinct Subpopulations of Raphe Serotonin Neurons. ACS Chemical Neuroscience. 2013; 4:200–209. [PubMed: 23336059]
35. Rylander D, Parent M, O'Sullivan SS, Dovero S, Lees AJ, Bezard E, et al. Maladaptive plasticity of serotonin axon terminals in levodopa-induced dyskinesia. Annals of Neurology. 2010; 68:619–28. [PubMed: 20882603]
36. Zhang Z, Kang il J, Vaucher E. Axonal varicosity density as an index of local neuronal interactions. PloS ONE. 2011; 6:e22543. [PubMed: 21811630]
37. Wierenga CJ, Schuemann A, Klawiter A, Bonhoeffer T, Wierenga CJ. Structural plasticity of GABAergic axons is regulated by network activity and GABAA receptor activation. Frontiers in Neural Circuits. 2013; 7:113. [PubMed: 23805077]
38. Hoover WB, Vertes RP. Anatomical analysis of afferent projections to the medial prefrontal cortex in the rat. Brain structure & Function. 2007; 212:149–79. [PubMed: 17717690]
39. Crawford LK, Craige CP, Beck SG. Glutamatergic input is selectively increased in dorsal raphe subfield 5-HT neurons: role of morphology, topography and selective innervation. European Journal of Neuroscience. 2011; 34:1794–1806. [PubMed: 22098248]
40. De-Miguel FF, Trueta C. Synaptic and Extrasynaptic Secretion of Serotonin. Cellular and Molecular Neurobiology. 2005; 25:297–312. [PubMed: 16047543]
41. Stettler DD, Yamahachi H, Li W, Denk W, Gilbert CD. Axons and synaptic boutons are highly dynamic in adult visual cortex. Neuron. 2006; 49:877–87. [PubMed: 16543135]
42. Paola V, Holtmaat A, Knott G, Song, Wilbrecht L, Caroni P, Svoboda K. Cell Type-Specific Structural Plasticity of Axonal Branches and Boutons in the Adult Neocortex. Neuron. 2006; 49:861–875. [PubMed: 16543134]
43. Hamani C, Diwan M, Isabella S, Lozano AM, Nobrega JN. Effects of different stimulation parameters on the antidepressant-like response of medial prefrontal cortex deep brain stimulation in rats. Journal of Psychiatric Research. 2011; 44:683–7. [PubMed: 20096858]
44. Li B, Piriz J, Mirrione M, Chung C, Proulx CD, Schulz D, et al. Synaptic potentiation onto habenula neurons in the learned helplessness model of depression. Nature. 2011; 470:535–9. [PubMed: 21350486]
45. Krishnan V, Han M, Graham D, Berton O, Renthal W, Russo S, et al. Molecular adaptations underlying susceptibility and resistance to social defeat in brain reward regions. Cell. 2007; 131:391–404. [PubMed: 17956738]
46. Kalueff A, Avgustinovich D, Kudryavtseva N, Murphy D. BDNF in anxiety and depression. Science. 2006; 312:1598–9. author reply 1598-9. [PubMed: 16778038]
47. Henn F. Circuits, cells, and synapses: toward a new target for deep brain stimulation in depression. Neuropsychopharmacology. 2012; 37:307–8. [PubMed: 22157873]

48. Montgomery E, Gale J. Mechanisms of action of deep brain stimulation (DBS). Neuroscience and Biobehavioral Reviews. 2008; 32:388–407. [PubMed: 17706780]

49. van Elburg RA, van Ooyen A. Impact of Dendritic Size and Dendritic Topology on Burst Firing in Pyramidal Cells. PLOS Computational Biology. 2010; 6:e1000781. [PubMed: 20485556]

50. Prange O, Wong TP, Gerrow K, Wang YT, El-Husseini A. A balance between excitatory and inhibitory synapses is controlled by PSD-95 and neuroligin. Proceedings of the National Academy of Sciences of the United States of America. 2004; 101:13915–20. [PubMed: 15358863]

51. Jankowski MP, Sesack SR. Prefrontal cortical projections to the rat dorsal raphe nucleus: Ultrastructural features and associations with serotonin and γ-aminobutyric acid neurons. The Journal of Comparative Neurology. 2004; 468:518–529. [PubMed: 14689484]

52. Vyas A, Mitra R, Rao BS, Chattarji S. Chronic stress induces contrasting patterns of dendritic remodeling in hippocampal and amygdaloid neurons. The Journal of Neuroscience. 2002; 22:6810–8. [PubMed: 12151561]

53. Paxinos, G.; Franklin, K. The Mouse Brain in Stereotaxic Coordinates. Second Edition. Academic Press; San Diego: 2001.

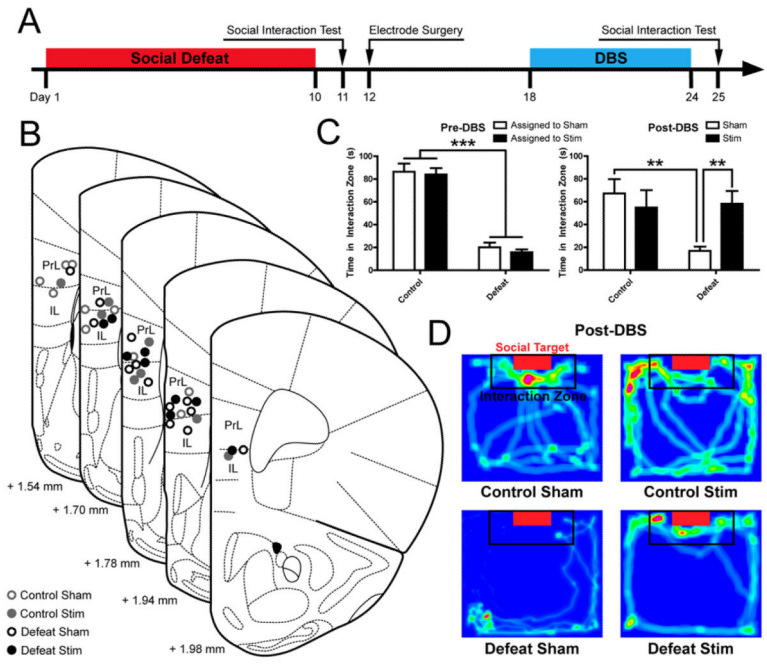

Figure 1. Chronic vmPFC DBS reverses sustained socioaffective deficits after defeat stress

(A) Experimental design: Mice were surgically implanted 48 hours after the conclusion of social defeat and left undisturbed for 7 days after surgery until the beginning DBS treatment. The antidepressant-like activity of vmPFC DBS was evaluated by comparing social interaction scores after 7 days of DBS (Day 25) to baseline interaction levels determined 24 h after the last social defeat episode (Day 11). **(B)** Verification of unilateral DBS electrodes placements in the left vmPFC of sham-stimulated mice (open circles) and stimulated mice (solid circles). Images from Paxinos and Franklin (53) and reprinted with permission from Elsevier. **(C)** Social defeat exposure induced a reduction in social interaction ($p < 0.001$, left panel) that was sustained in sham mice until Day 25 ($p < 0.01$ Day 25 Control Sham *vs.* Defeat Sham). Seven days of DBS resulted in a complete restoration of social interaction in defeated mice ($p < 0.01$, right panel), while there was no significant effect of DBS on social interaction in unstressed controls ($p > 0.05$, Day 25 Control Sham *vs.* Control Stim). n = 8-13 mice per condition. **(D)** Representative heat maps illustrating mouse movements relative to social target in each experimental condition. Hot colors indicate locations where the mice spent the most time. Significant differences are indicated by $*p < 0.05$, $**p < 0.01$, $***p < 0.001$.

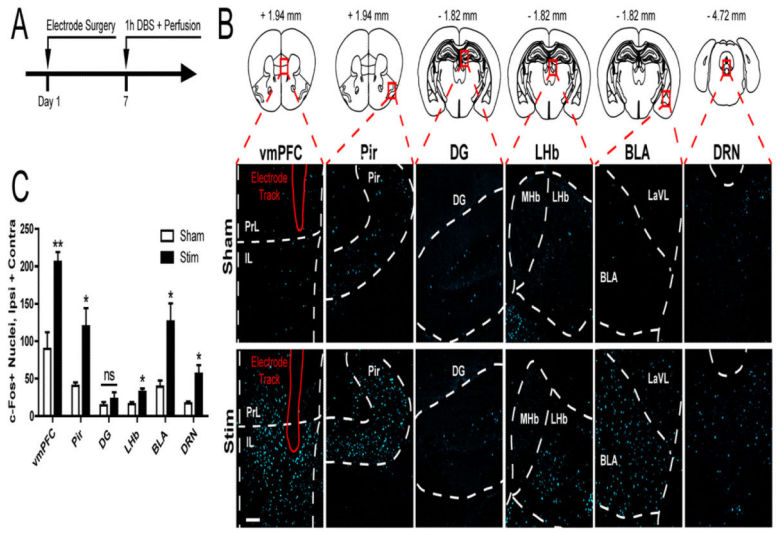

Figure 2. Acute DBS induces neural activation of afferent and efferent monosynaptic connections to the vmPFC

(A) Experimental design. Mice were implanted with unilateral DBS electrodes in the left vmFPC, allowed to recover for 7 days, and underwent DBS for 1 hour immediately followed by perfusion. **(B)** Representative images of c-Fos immunoreactivity in the vmPFC, Anterior Piriform Cortex (Pir), Dentate Gyrus (DG), Lateral Habenula (LHb), Basolateral Amygdala (BLA) and Dorsal Raphe Nucleus (DRN). Scale bar, 100 μm. Images from Paxinos and Franklin (53) and reprinted with permission from Elsevier. **(C)** Corresponding counts of the number of c-Fos^{+} nuclei revealed significant increases with DBS locally at the stimulation site (vmPFC) and in distal regions known to either receive (LHb, BLA, DRN) and/or send (Pir, BLA, DRN) projections to the vmPFC. In contrast, minor changes were seen in the DG, which has no known monosynaptic connection to the vmPFC. n = 3-4 per condition. Significant differences are indicated by *$p < 0.05$, **$p < 0.01$.

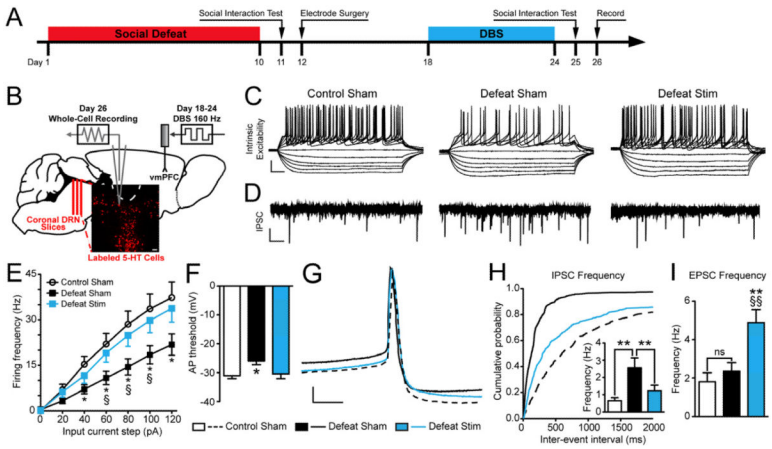

Figure 3. Chronic vmPFC DBS reverses social defeat-induced hypoexcitability and restores levels of inhibitory input onto DRN 5-HT neurons

(A) Experimental timeline. **(B)** Schematic depicting electrophysiology protocol; coronal DRN slices were collected from *Pet1-tdTomato* mice 48 h following DBS and whole-cell recordings were performed from fluorescently identified 5-HT neurons in the ventromedial DRN. Images from Paxinos and Franklin (53) and reprinted with permission from Elsevier. **(C)** Raw data traces depicting changes in membrane potential of DRN 5-HT neurons in response to 20 pA steps of depolarizing current. Scale bar, 25 mV, 50 ms. **(D)** Representative traces depicting spontaneous IPSC activity in DRN 5-HT neurons. Scale bar 20 pA, 1 s. **(E)** Frequency-current plots show a decrease in intrinsic excitability of DRN 5-HT neurons in defeated mice (*$p < 0.05$, 40-120 pA). Hypoexcitability of DRN 5-HT neurons is reversed in defeated mice treated with chronic DBS ($^{§}p < 0.05$, 60-100 pA); intrinsic excitability is comparable to that of controls [$N(n)$ = 2 mice (20 cells) for Control Sham, 4(23) for Defeat Sham, 3(20) for Defeat Stim]. **(F)** The action potential threshold of DRN 5-HT neurons is increased by social defeat ($p < 0.05$) and restored after vmPFC DBS. **(G)** Enlarged depiction of individual action potentials in DRN 5-HT neurons for each experimental condition. Scale bar 10 mV, 5 s. **(H)** Cumulative probability plots displaying the defeat-induced shift to shorter inter-event intervals of spontaneous IPSC's in DRN 5-HT neurons versus controls. DRN 5-HT neurons in DBS-treated mice display a shift back towards longer inter-stimulus intervals ($p < 0.001$). Inset: summary histogram showing increased mIPSC frequency after CSDS that is reversed after vmPFC DBS [$N(n)$ = 2(14) for Control Sham, 4(19) for Defeat Sham, 3(16) for Defeat Stim]. **(I)** Spontaneous EPSC frequency of DRN 5-HT neurons is unchanged in defeated mice but increased in defeated mice treated with vmPFC DBS ($^{§§}p < 0.01$ *vs.* Control Sham, **$p < 0.01$ *vs.* Defeat Sham). Significant differences are indicated by *$p < 0.05$, $^{§}p < 0.05$, $^{§§}p < 0.01$, **$p < 0.01$.

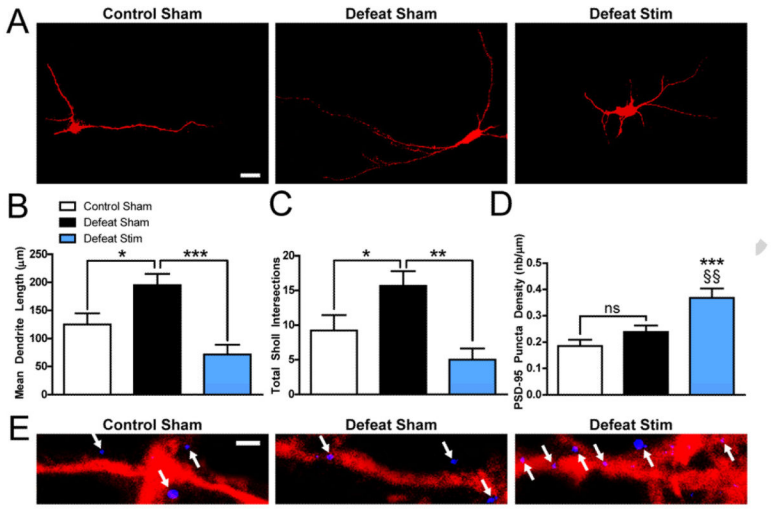

Figure 4. Chronic vmPFC DBS reverses social defeat-induced dendritic plasticity in DRN 5-HT neurons

(A) Representative images of biocytin-filled 5-HT neurons. Scale bar, 30µm. **(B)** Social defeat induces a significant increase in dendritic length ($p < 0.05$), and chronic DBS restores mean dendrite length ($p < 0.001$) to levels comparable to controls ($p > 0.05$). **(C)** Social defeat induces a significant increase in dendritic complexity as assayed by Sholl analysis ($p < 0.05$), and chronic DBS restores dendritic complexity ($p < 0.01$) to levels comparable to controls ($p > 0.05$) [$N(n)$ = 2 mice (13 cells) for Control Sham, 4(18) for Defeat Sham, 2(10) for Defeat Stim]. **(D)** Social defeat does not significantly change the density of PSD-95 puncta along 5-HT DRN dendrites ($p > 0.05$ Control Sham *vs.* Defeat Sham), while DBS significantly increases PSD-95 puncta density (***$p < 0.001$, Control Sham *vs.* Defeat Stim, $^{§§}p < 0.01$, Defeat Sham *vs.* Defeat Stim) [$N(n)$ = 2 mice (16 dendritic segments) per condition]. **(E)** Representative images of PSD-95 puncta along 5-HT DRN dendrites. Scale bar, 1.00 µm. Significant differences are indicated by *$p < 0.05$, **$p < 0.01$, $^{§§}p < 0.01$, ***$p < 0.001$.

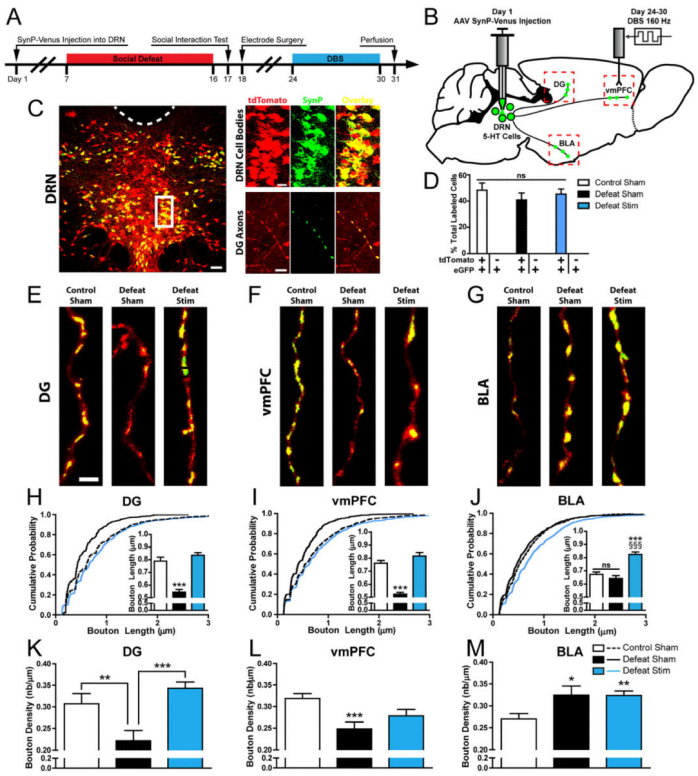

Figure 5. Social defeat and chronic vmPFC DBS induce structural axonal plasticity in DRN 5-HT neurons

(A) Experimental design: An AAV vector carrying a Flex Synaptophysin-Venus (SynP-Venus) cassette was injected into the DRN of *Pet1-tdTomato* mice. Mice underwent the same social defeat and DBS paradigm as described in Figure 1 and were perfused 24 h after the end of stimulation. **(B)** Experimental schematic indicating AAV injection in the DRN, resulting in targeting of the SynP-Venus fusion protein to 5-HT cell bodies in the DRN and labeling of presynaptic boutons in DRN projection regions such as the dentate gyrus (DG), vmPFC, and basolateral amygdala (BLA). Images from Paxinos and Franklin (53) and reprinted with permission from Elsevier. **(C)** Left Panel: Low magnification confocal image illustrating SynP-Venus expression (green) in the DRN of *Pet1-tdTomato* mice. 5-HT neurons are genetically identified by expression of the tdTomato reporter (red). Colocalization of SynP-Venus and tdTomato is indicated by yellow. Right Panel: High magnification images illustrate SynP-Venus localization to 5-HT somas in the DRN (top) and 5-HT axon terminals in the DG (Bottom). Note the concentration of SynP-Venus signal to axonal boutons. Scale bars: 50 µm (left), 20 µm (top right) 5 µm (bottom left). **(D)** Validation of SynP-Venus expression efficiency and selectivity. Over 40% of all tdTomato$^+$ DRN somas expressed SynP-Venus, indicating strong transduction efficiency, and >99% of all SynP-Venus$^+$ DRN somas were tdTomato$^+$, indicating complete serotonergic selectivity. There were no significant differences in transduction rates between Control Sham, Defeat Sham, and Defeat Stim mice ($p > 0.05$). **(E-G)** Representative images of DRN 5-HT axons in the DG, vmPFC, and BLA across treatment groups. Scale bar, 2 µm. Morphometric measures of 5-HT presynaptic bouton length **(H-J)** and density **(K-M)** were derived from intensity measurements of SynP-Venus fluorescence intensity along tdTomato$^+$ traced axons

segments (see Figure S3 for example of analysis). Social defeat significantly reduced the length and density of presynaptic boutons in the DG and vmPFC while increasing the density of presynaptic boutons in the BLA. DBS restored the length and/or density of 5-HT presynaptic boutons in the DG and the vmPFC to the level of unstressed controls and increased bouton length over the level of controls in the BLA. Bouton Length: n = 291-1362 boutons per condition from 2 mice per condition, Bouton Density: n = 31-66 axons from 2 mice per condition. Significant differences are indicated by $*p < 0.05$, $**p < 0.01$, $***p < 0.001$.